

Shape Estimation and Prediction of Locations of the Force on a Flexible Tube using Strains at a Few Points

Ananya, Shanthanu Chakravarthy, Kumar Saurabh and G. K. Ananthasuresh

Abstract

In this work, we address two problems concerning flexible tubes such as the ones used in endoscopy. In the first problem, we use a shape estimation algorithm to simulate the shape of the entire endoscope during endoscopy. In the second problem, we explore a method to predict the location of point forces acting on the tube during endoscopy. Strain measurements made at a few discrete locations on the tube are used as input for both shape estimation and force-location prediction.

A suitable strain interpolation method is explored to capture all the necessary information for the aforementioned two problems. For the first problem, we implemented in both 2D and 3D a shape estimation algorithm based on differential geometry methods. Through experiments we show that the developed shape estimation method can reconstruct the shape with errors no more than 20%. For the second problem, we look at the nature of the derivatives of the interpolated strain values. As the derivative of the strain is proportional to the shear force, we identify the locations of the applied point forces by looking for discontinuities in the strain derivative. Furthermore, we develop graphical visualisation method using OpenGL libraries to render the shape of the endoscope in real time. Implementation and error analysis of the shape estimation algorithm, validation of the force-location predicting method, and the visualisation module comprise the paper.

Keywords: Endoscopy, Endoscopic simulator, Strain interpolation.

1 Introduction

In this paper, we present a shape estimation method for endoscopy using strain measurements. We also explore a method to predict the location of the point forces on the endoscope.

Ananya

Department of Mechanical Engineering, Indian Institute of Science, Bengaluru, E-mail: ananya@mecheng.iisc.ernet.in.

Shanthanu Chakravarthy (Corresponding Author)

Department of Mechanical Engineering, Indian Institute of Science, Bengaluru, E-mail: sc@mecheng.iisc.ernet.in.

Kumar Saurabh

Department of Instrumentation and Applied Physics, Indian Institute of Science, Bengaluru, E-mail: kumar.saurabh@iap.iisc.ernet.in

G. K. Ananthasuresh

Department of Mechanical Engineering, Indian Institute of Science, Bengaluru, E-mail: suresh@mecheng.iisc.ernet.in.

Endoscopy is a minimally invasive procedure where a flexible tube is inserted through the digestive tract for medical examination, and lately also for surgical procedures [1]. The flexible tube is referred to as an endoscope. Fig. (1a) shows an illustration of the endoscope. Physicians performing endoscopy rely on the view from the camera attached to the distal end of the endoscope and the intuition of the shape information for manipulating endoscope inside the Gastrointestinal (GI) tract. During endoscopy, there is a chance of prodding the stomach surface too hard leading to discomfort and injuries to the patient. The endoscope also tends to loop inside the stomach requiring the physician to 'shorten the scope length' while performing the procedure [2, 3].

Fluoroscopy is a commonly used technique for visualizing the endoscope inside the GI-tract [4]. A fluoroscopy image obtained during one such procedure is shown in Fig. (1b). Fluoroscopy is an imaging technique that uses X-rays to obtain real-time moving images of the internal structures of a patient through the use of a fluoroscope. In [5], Adler notes the shortcomings of fluoroscopy: "Proficient use of fluoroscopic hardware requires skill and practice". Furthermore, radiation exposure is not advisable and has to be minimised [6]. Owing to these problems, a real-time non-invasive endoscope visualisation system that does not use radiation would greatly aid in endoscopy.

Shape estimation system developed in this work has the potential to provide a complete view of the endoscope as the procedure is being performed. Furthermore, this shape estimation module will complement a virtual reality-based endoscopic simulator with haptic feedback [7, 8]. In a training simulator, it is important to guide the trainee to perform effective movements of the endoscope [9-12]. Test cases can be created by recording the path followed by the endoscope while a skilled operator is performing the procedure. These test cases can be used to train the novice gastroenterologists. In addition, the haptic system would greatly benefit from real force and position measurement data.

It is reasonable to assume that forces exist on the endoscope inserted into the GI tract only at the points where the endoscope touches the walls of the GI tract. In view of this, we attempt to predict the location of forces based on the strain information. With this method, force and its location information can be estimated from a real endoscopy procedure. With the knowledge of the forces and their locations, the simulator will be able to effectively replicate the forces as in a real endoscopy. Computation of the magnitudes of the forces applied on a flexible tube undergoing very large displacements is presented [13].

Strain acquisition during endoscopy has to be done non-intrusively. Piezoresistive strain gauges require external wiring and tend to be bulky. Fiber Bragg Grating (FBG) sensors are most suited for this application due to their small size (about 250 microns including the plastic jacket) as well as their non-electric nature. Deformation sensing method using FBG sensor net to get a real-time display during colonoscopy was discussed by Yi et al. [14] The sensor net is embedded into the biopsy channel of the endoscope and from the wavelength shift of the FBG, strains at the grating locations on the endoscope can be estimated. The strain measured at discrete locations are used to estimate the shape of the endoscope.

Techniques to interpolate the discrete strain values are available [15, 16]. Cubic spline interpolation is used in this work, as they gave us good interpolation without oscillations. For shape reconstruction, considering large deformations, beam model is used to extract curvatures from strain data. Finally, 2D and 3D shape reconstruction methods that are based on differential geometry are discussed.

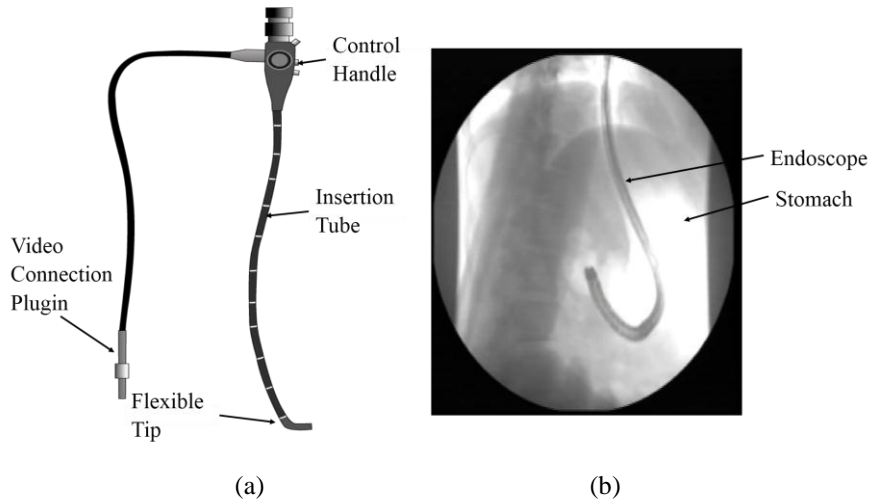


Figure 1: (a) Illustration of the endoscope (b) Profile of the endoscope with fluoroscopy.

To predict the location of forces on the endoscope, we look at nature of strain along the length of endoscope. Non-differential points (cusps) in the interpolated strain indicate the locations of point forces because the derivative of the strain in a beam is proportional to the shear force. Therefore, we use and compare both cubic spline interpolation and Chebyshev interpolation techniques for capturing the cusps in strain values.

In the remainder of the paper is organised as follows. We give an overview of the strain acquisition system in Section 2. The strain interpolation method is discussed in Section 3. This is followed by Section 4 in which the shape reconstruction algorithms are presented. Section 5 briefly describes the visualization method. In Section 6, a method to predict the location of forces on the endoscope tube is developed. Concluding remarks are in Section 7.

2 Shape Estimation

Shape estimation method has three major steps. The first step involves strain acquisition by measuring discrete strain values along the endoscope. This is followed by the interpolation step where the measured strains are interpolated along the length of the endoscope. The final step is the shape reconstruction algorithm that estimates the shape of the endoscope.

2.1 Strain acquisition

In this work, strain acquisition is explored using both FBG sensors and strain gauges. Fig. (2b) shows the setup for strain measurement using FBG sensors. It consists of an interrogator coupled with a data acquisition system that reads the frequency shift in real time. Laser light is sent through the optical fiber that is etched with gratings at certain intervals along its length [17]. Up to eight sensors can be written on a single optic fiber at 10 cm interval, allowing strains to be measured at eight discrete locations. Four such optical fibers can be placed along the periphery to obtain strains in four

different directions, as shown in Fig. (2a). Sensors were written on the optical fiber using a mask and Krypton Fluoride (KrF) laser [18].

In our preliminary experiments, the sensors were directly bonded onto the endoscope. However, the neutral axis is not at the center of the endoscope and the strains will be different for bending in different directions. Also, the rubber tubing at the surface may not transfer actual strain based on bending theory. As seen in Table 1, the errors in curvature estimation are very high in this configuration. Hence, we bonded the sensor onto a nitinol (a nickel titanium alloy) wire. The dimension of the nitinol wire (1.2 mm) is small enough to be passed through the biopsy channel of the endoscope. This gave good results for curvature estimation as shown in Table 1.

Bonding the sensors on the wire is not easy as the fragile FBG sensors tend to break. We are exploring other methods of bonding the sensors to facilitate ease of handling and operation. Hence, although FBG sensors are most suited for shape estimation application, strain gauges are used in this work for the experiments. Strain gauges are robust and easy to handle in ex vivo experiments.

2.2 Strain Interpolation

Strain is measured at discrete points (typically around five to eight) along the length of the endoscope. A good shape reconstruction algorithm requires the interpolated values all along the length of the scope. Higher order interpolation using a global polynomial often exhibits oscillations leading to errors. From our experiments with

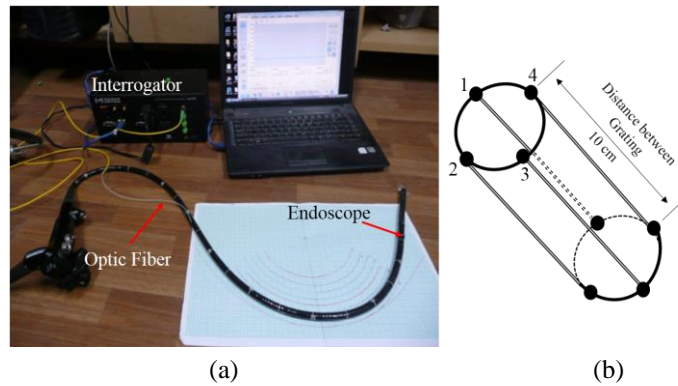


Figure 2: (a) Experimental setup to measure strain using FBG sensor. (b) Four optical fibers with gratings at regular intervals.

Table 1: Estimated strains and bending radii with FBG sensors

	<i>Actual Radius of Curvature (mm)</i>	<i>Measured Strain (μstrain)</i>	<i>Calculated Radius of Curvature (mm)</i>	<i>Error (%)</i>
<i>Mounted on the endoscope</i>	164	3600	1404	756
	130	4000	1247	859
	96	4900	1012	954
<i>Mounted on nitinol</i>	164	3800	158	-3.6
	154	4100	147	-4.5
	141	4600	130	-7.8

strain data, cubic splines showed reduced oscillations and interpolated strains with good accuracy. While higher order polynomials were considered to ensure a degree of smoothness, it was seen that quartic or higher order splines exhibit instabilities. Therefore, we employ cubic splines to interpolate strain values. We refrained from using in-built functions and implemented the interpolation method in both MATLAB and VC++. This gave us better control over the data and allowed us to readily use the interpolation method with other aspects of the shape estimation method.

We fit a system of cubic spline for the strain $\varepsilon_1, \varepsilon_2, \dots, \varepsilon_n$ given at n points x_1, x_2, \dots, x_n . Here, x is the position along the endoscope.

Cubic spline for any point x is given as

$$\varepsilon_j(x) = \alpha_j + \beta_j(x - x_j) + \gamma_j(x - x_j)^2 + \delta_j(x - x_j)^3 \quad x_j \leq x \leq x_{j+1} \quad (1)$$

where $j = 1, 2, \dots, n-1$

We use the properties of the cubic spline:

- ε_j interpolates all data points, so $\varepsilon_j(x_j) = \hat{\varepsilon}_j = \alpha_j$ for $j = 1, 2, \dots, n-1$
- The cubic spline is continuous at interior points, $\varepsilon_{j+1}(x_j) = \varepsilon_j(x_j)$ for $j = 1, 2, \dots, n-2$
- The function has first order continuity, $\varepsilon_{j+1}'(x_j) = \varepsilon_j'(x_j)$ for $j = 1, 2, \dots, n-2$
- The function has second order continuity, $\varepsilon_{j+1}''(x_j) = \varepsilon_j''(x_j)$ for $j = 1, 2, \dots, n-2$

We compute a cubic spline by calculating the coefficients $(\alpha_j, \beta_j, \gamma_j, \delta_j)$ for $1 \leq j \leq (n-1)$.

2.3 Shape Reconstruction

A 2D algorithm using circular arc segments and a 3D algorithm using helical arc segments are developed as a part of shape reconstruction using curvature. Curvature information for each finite segment of the endoscope can be obtained from the strain based on the beam model.

$$\rho = y / \varepsilon \quad (2)$$

where ρ is the radius of curvature, y is the distance of the sensor from the neutral plane, and ε the strain in the segment.

2.3.1 2D method using circular arc segments

Endoscope shape can be reconstructed by marching from point (x_i, y_i) to point (x_{i+1}, y_{i+1}) along the length of the endoscope as shown in Fig (3). In the 2D case, the length of the endoscope is divided into finite segments, dL . Each segment is considered to be a circular arc of radius equal to the radius of curvature, ρ . The angle subtended by the arc segment is given by

$$d\phi = dL / \rho \quad (3)$$

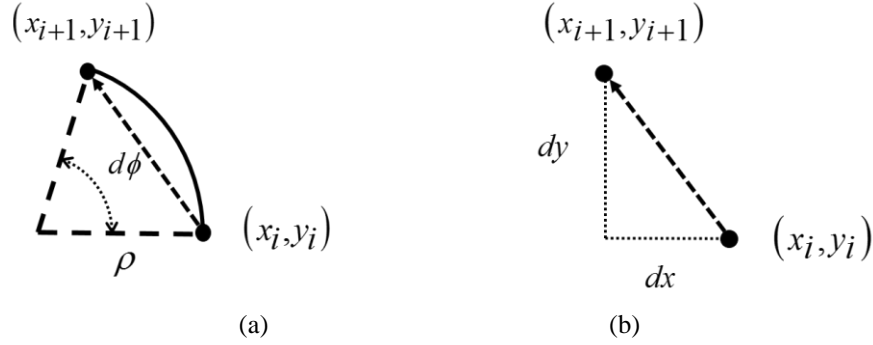


Figure 3: Model of 2D shape reconstruction. (a) Circular arc sections depicting central angle corresponding to the strain, (b) Marching increments based on differential geometry.

where dL = length of segment. The successive increments along the x-axis and the y-axis are given by

$$\begin{aligned} dx &= \rho \sin(d\phi) \\ dy &= \rho(1 - \cos(d\phi)) \end{aligned} \quad (4)$$

Piecewise integration can be carried out along the length of the beam to compute x , y and ϕ . However, Eqs. (3) and (4) assume that $d\phi$ is measured from zero angle. This is not true for successive segments along the length. Therefore, we rotate dx and dy by $d\phi_{sum}$, which is the sum of $d\phi$ up to the previous segments. The new points (x_{i+1}, y_{i+1}) are computed as

$$\begin{bmatrix} x_{i+1} \\ y_{i+1} \end{bmatrix} = \begin{bmatrix} x_i \\ y_i \end{bmatrix} + R_z(d\phi_{sum}) \begin{bmatrix} dx \\ dy \end{bmatrix} \quad (5)$$

In order to verify the 2D algorithm, standard parametric curves were used. Curvature was obtained from the parametric equation of the curve. This was used in lieu of strain to construct the shape. Fig. (4) compared the reconstructed shapes for some representative curves. This method works well for any 2D curve and is fast as it takes less than 0.05 s for any 2D curve.

2.3.2 3D method using helical segments

In the 3D case, the curve is assumed to be made up of helical arc segments. We use the property of the helix which has constant curvature and constant torsion. We obtain these torsion and curvature values from the corresponding strain values. Our approach is to march from point \mathbf{P}_i to \mathbf{P}_{i+1} by considering this to be a helical segment.

A point in the helical segment can be defined by

$$\mathbf{P} = (\rho \cos \theta, \rho \sin \theta, c\theta) \quad (6)$$

where,

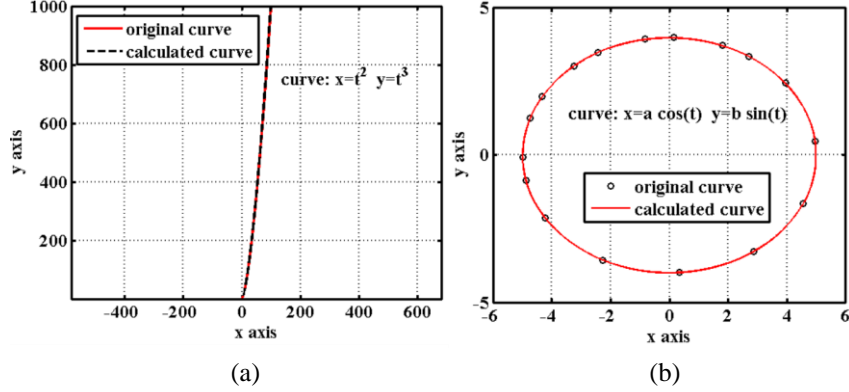


Figure 4: Parametric 2D curves. (a) $x = t^2, y = t^3$, (b) $x = a \cos t, y = b \sin t$

$$\rho = \frac{\kappa}{\kappa^2 + \tau}, \quad \theta = \frac{dL}{\sqrt{\rho^2 + c^2}}, \quad c = \frac{\tau}{\kappa^2 + \tau} \quad (7)$$

where κ is the curvature, τ is the torsion and dL is the length of the segment.

Eq. (6) is valid for helical segment with origin as the center and Z- axis as the axis of the helix. However, each helical segment in shape re-construction has a different center and axis of rotation. We find the center of the helical segment by marching along the normal, \mathbf{N} from point \mathbf{P}_i by a distance equal the radius of curvature, ρ . As shown in Fig. (5), a local co-ordinate system is created at this center, \mathbf{C}_i .

Now, to find the axis of the helix we observe that the tangent, \mathbf{T} of the helix makes a constant angle with the axis of the helix. This angle ϕ is given by

$$\phi = \cos^{-1} \left(\frac{c}{\sqrt{\rho^2 + c^2}} \right) \quad (8)$$

Therefore, we can find the axis of the helix by rotating the tangent \mathbf{T} by an angle ϕ in the clockwise direction about the normal, \mathbf{N} . Now we draw the helical segment in the local coordinate system and transform the helical segment to the global coordinate system. The new point \mathbf{P}_{i+1} in the global coordinate system is given by

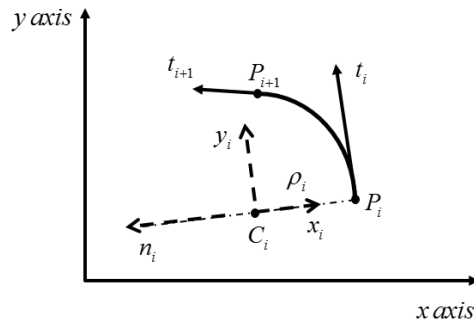


Figure 5: Marching from P_i to P_{i+1} for 3D reconstruction.

$$\mathbf{P}_{i+1} = \mathbf{R} \mathbf{P}_i + \mathbf{C}_i \quad (9)$$

where \mathbf{R} is the rotation matrix to transform the point from local coordinate system to global coordinate system.

The algorithm is used to reproduce a standard curves from their parametric curvature and torsion as shown in Fig. (6). The RMS error corresponding to the reconstruction algorithm is always observed to be less than 0.01.

2.4 Visualization

The reconstruction algorithm is interfaced with an interactive visualisation platform using OpenGL libraries. OpenGL interface is used to graphically render the calculated shape. It is coupled with VC++ and can be interfaced with the other aspects of the simulator. With OpenGL, we build the desired model using geometric primitives like points and lines. We can also render the desired texture to the visualisation. The interactive platform has a console window to input strain values. Fig. (7) shows one such visualisation with the virtual model of the stomach.

2.5 Experiments

The shape estimation system developed in this work is verified using experiments using strain gauges. The strain gauge is embedded on a spring steel strip of thickness 0.5 mm. Four strain gauges (350Ω , Gauge factor = 1.3) are mounted on the strip at regular intervals. A Wheatstone bridge network with the strain gauge as one of its arms

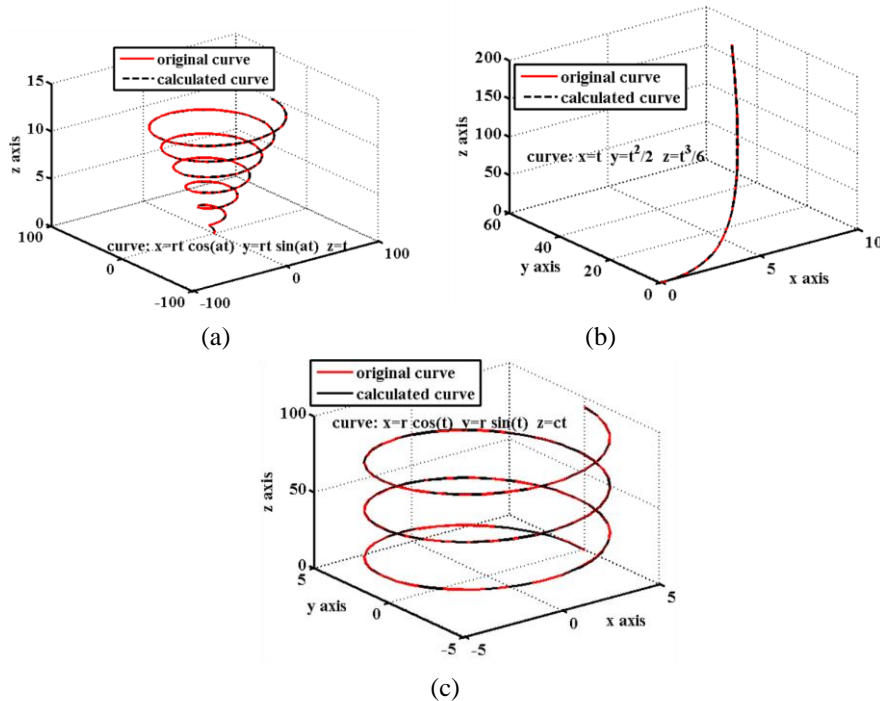


Figure 6: Parametric 3D curves. (a) $x = rt \cos t, y = rt \sin t, z = t$, (b) $x = t, y = \frac{t^2}{2}, z = \frac{t^3}{6}$, (c) $x = r \cos t, y = r \sin t, z = ct$

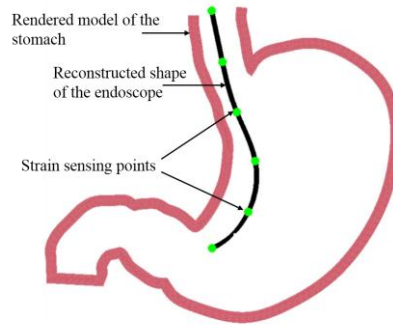


Figure 7: Graphical rendering of the endoscope inside the stomach.

is constructed. dSPACE is used for data acquisition and voltage-to-strain conversion. Measured strain was integrated into the visualization algorithm. Fig. (8) shows one such experiment and the visualization of the reconstructed shape.

3 Location of Point Forces on the Tube

Our research question is to find the location of point forces on the endoscope given the discretely measured strain values. We hypothesize that the location of forces can be predicted by looking at the nature of the strains and their derivatives. Fig. (9a) shows the FEA simulations and the strain along the length of a fixed-fixed beam. In line with our hypothesis, non-differentiable points can be seen at force locations along the length of the beam (Fig. (9b)). We verified this for different boundary conditions (fixed-fixed, fixed-pinned, pinned-pinned, and pinned-fixed). These non-differentiable points are also seen in fixed-free boundary condition as shown in Fig. (10).

In actual implementation, we measure strain at discrete locations and interpolation is employed to obtain strain all along the length of the endoscope. However, interpolation has the effect of smoothening the strain data and we will not be able to observe non-differentiable points. Because of this, looking at cusps to identify a possible force location is appropriate. Here, we study the two interpolation methods, cubic spline and Chebyshev interpolation at effectively capturing the cusps.

While in cubic spline interpolation the interpolating nodes are equidistant, in Chebyshev interpolation the interpolation points correspond to the Chebyshev nodes.

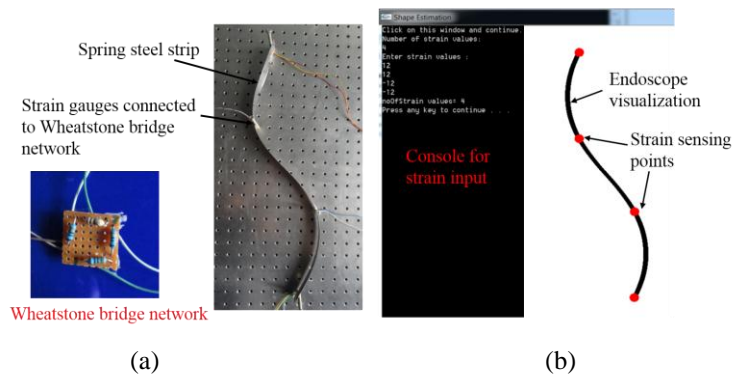


Figure 8: (a) Steel strip with four strain gauges connected to Wheatstone bridge network. (b) Visualization of the reconstructed shape together with console window.

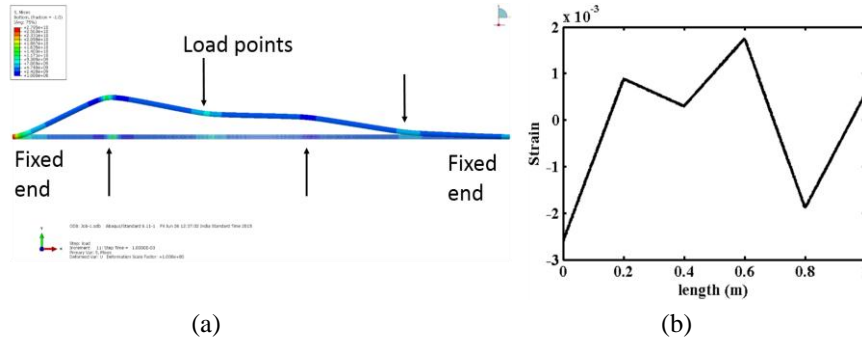


Figure 9: (a) Profile of the fixed-fixed beam in Abaqus with 4 point loads, (b) Strain distribution along the length of the beam.

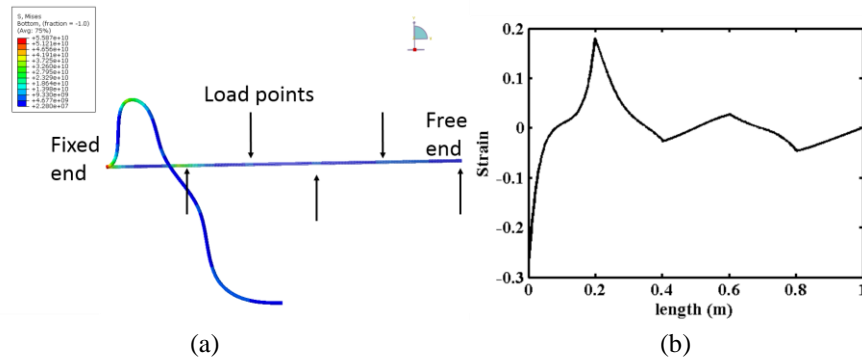


Figure 10: (a) Profile of the fixed-free beam in Abaqus with 5 point loads, (b) Strain distribution along the length of the beam.

The Chebyshev nodes are selected in such a way as to provide a smooth interpolation while avoiding oscillations [19]. Fig. (11) shows the comparison of the two interpolation methods with finite element modality in Abaqus (www.simulia.com).

When interpolating with fewer points, cubic spline performs relatively better. However, we see from Fig. (12) that with increased interpolating points, both the methods are reasonably good in capturing the cusps. The location of the cusps do not exactly match the location of the forces. However, they are relatively close and give an intuitive idea about the location of the forces. Furthermore, we observe that some of the Chebyshev nodes coincide with the location of the forces. These observations were consistent for different boundary conditions (pinned-pinned, pinned-fixed, and fixed-pinned).

4 Closure

In this paper, we presented a shape estimation system for endoscopy and a method to predict the location of forces. Shape estimation method was presented together with strain experiments. The shape reconstruction algorithms was shown to reconstruct shapes with RMS error less than 0.01. Experimental verification together with graphical visualization was demonstrated. In the second part of the paper, we looked at two interpolation methods to identify maxima and minima in strain data. We observed that increased number of interpolating points give insights into the location of forces. As part of the future course of this work, we are looking at iterative methods to find the location of forces on the endoscope. Integration of FBG sensor net with the

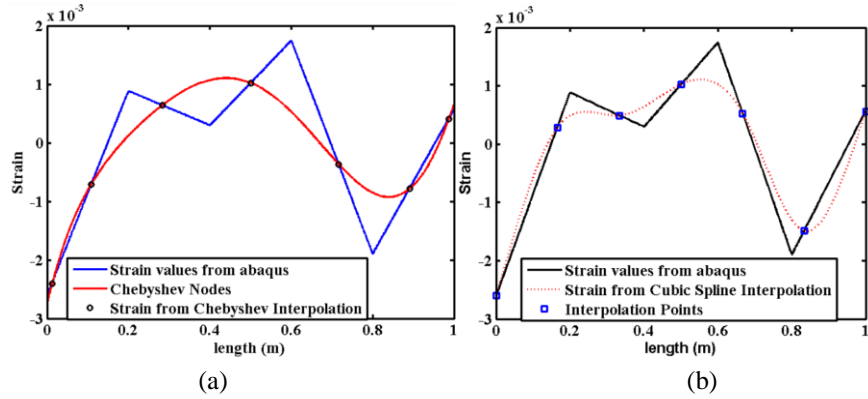


Figure 11: Strain interpolated at 7 points. (a) Strain plot from Chebyshev interpolation, (b) Strain plot from cubic spline interpolation.

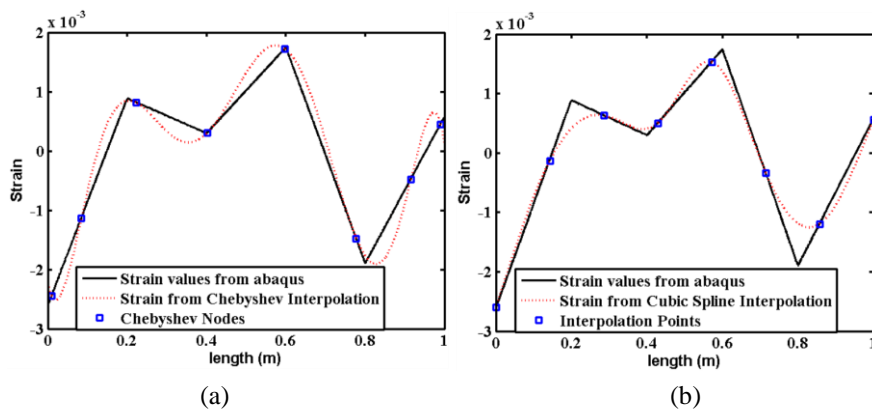


Figure 12: Strain interpolated at 8 points. (a) Strain plot from Chebyshev interpolation, (b) Strain plot from cubic spline interpolation.

proposed estimation system and in-vivo experiments will also be pursued in the extension of this work.

Acknowledgement

This work was financially supported by the by the Robert Bosch Centre for Cyber Physical Systems (RBCCPS) at the Indian Institute of Science (IISc), Bangalore. Clinical guidance was provided by Dr. Pradeep Rebala, Dr. Nageswar Reddy, and Dr. G.V. Rao at the Asian Institute of Gastroenterology, Hyderabad. Authors thank Sreenath Balakrishnan for helpful discussions on shape reconstruction algorithm.

References

- [1] R. Hart and M. Classen, "Complications of diagnostic gastrointestinal endoscopy," *Endoscopy*, vol. 22, pp. 229-233, 1990.
- [2] J. Wang, L. Zhang, and W. Wu, "Current progress on natural orifice transluminal endoscopic surgery (NOTES)," *Frontiers of medicine*, vol. 6, pp. 187-194, 2012.

- [3] R. Couper, D. Moore, and G. Davidson, "Requirements for training to ensure competence of endoscopists performing invasive procedures in children," *Journal of pediatric gastroenterology and nutrition*, vol. 26, pp. 363, 1998.
- [4] W. C. Cirocco and L. C. Rusin, "Confirmation of cecal intubation during colonoscopy," *Diseases of the colon & rectum*, vol. 38, pp. 402-406, 1995.
- [5] D. G. Adler, "The Role of Fluoroscopy in the Endoscopic Management of Luminal Gastrointestinal Disorders," *Techniques in Gastrointestinal Endoscopy*, vol. 9, pp. 189-194, 2007.
- [6] W. B. Cheng, M. A. Moser, S. Kanagaratnam, and W. J. Zhang, "Overview of upcoming advances in colonoscopy," *Digestive endoscopy*, vol. 24, pp. 1-6, 2012.
- [7] S. Chakravarthy, K. Avinash, G. Ramu, and G. Ananthasuresh, "Design of an Endoscopic Haptic Display System using an Integrated Ring-actuator," presented at iNaCoMM, IIT Roorkee, 2013.
- [8] S. Chakravarthy, A. Rao, and G. Ananthasuresh, "A Haptic Simulator for Upper Gastrointestinal Endoscopy," presented at The Hamlyn Symposium on Medical Robotics, 2014.
- [9] E. Samur, L. Flaction, and H. Bleuler, "Design and evaluation of a novel haptic interface for endoscopic simulation," *Haptics, IEEE Transactions on*, vol. 5, pp. 301-311, 2012.
- [10] J. W. Peifer, W. D. Curtis, and M. J. Sinclair, "Applied virtual reality for simulation of endoscopic retrograde cholangio-pancreatography (ERCP)," *Studies in health technology and informatics*, vol. 29, pp. 36-42, 1995.
- [11] K. Ikuta, M. Takeichi, and T. Namiki, "Virtual endoscope system with force sensation," presented at Robotics and Automation, 1999. *Proceedings. 1999 IEEE International Conference on*, 1999.
- [12] O. Körner and R. Männer, "Implementation of a haptic interface for a virtual reality simulator for flexible endoscopy," presented at Haptic Interfaces for Virtual Environment and Teleoperator Systems, 2003. *HAPTICS 2003. Proceedings. 11th Symposium on*, 2003.
- [13] A. K. Nittala, S. Chakravarthy, and G. K. Ananthasuresh, "Real-time Large-deformation Modelling of a Flexible Endoscope Tube using Elastic Similarity ": *iNaCoMM*, 2015.
- [14] Y. Xinhua, W. Mingjun, and C. Xiaomin, "Deformation sensing of colonoscope on FBG sensor net," *TELKOMNIKA Indonesian Journal of Electrical Engineering*, vol. 10, pp. 2253-2260, 2012.
- [15] M. E. Mortenson, *Geometric modeling*: Industrial Press, Inc., 2006.
- [16] E. Kreyszig, *Differential Geometry (Dover Books on Mathematics)*: Dover Publications Inc., 1991.
- [17] R. S. Bhamber, T. Allsop, G. Lloyd, D. Webb, and J. D. Ania-Castanon, "Real-time 3D shape sensing and reconstruction scheme based upon fibre optic Bragg gratings," presented at Bragg Gratings, Photosensitivity, and Poling in Glass Waveguides, 2012.
- [18] A. D. Kersey, M. A. Davis, H. J. Patrick, M. LeBlanc, K. Koo, C. Askins, M. Putnam, and E. J. Friebele, "Fiber grating sensors," *Journal of lightwave technology*, vol. 15, pp. 1442-1463, 1997.
- [19] J. Mathews and K. Fink, *Numerical Methods Using MATLAB*: Pearson, 2004.